Ab-initio self-consistent Gorkov-Green's function calculations of semi-magic nuclei II. Numerical implementation at second order with a two-nucleon interaction

V. Somà,[1,2,*] C. Barbieri,[3,†] and T. Duguet[4,5,‡]

[1] *Institut für Kernphysik, Technische Universität Darmstadt, 64289 Darmstadt, Germany*
[2] *ExtreMe Matter Institute EMMI, GSI Helmholtzzentrum für Schwerionenforschung GmbH, 64291 Darmstadt, Germany*
[3] *Department of Physics, University of Surrey, Guildford GU2 7XH, UK*
[4] *CEA-Saclay, IRFU/Service de Physique Nucléaire, 91191 Gif-sur-Yvette, France*
[5] *National Superconducting Cyclotron Laboratory and Department of Physics and Astronomy, Michigan State University, East Lansing, MI 48824, USA*

(Dated: October 29, 2013)

The newly developed Gorkov-Green's function approach represents a promising path to the *ab initio* description of medium-mass open-shell nuclei. We discuss the implementation of the method at second order with a two-body interaction, with particular attention to the numerical solution of Gorkov's equation. Different sources of theoretical error and degrees of self-consistency are investigated. We show that Krylov projection techniques with a multi-pivot Lanczos algorithm efficiently handle the growth of poles in the one-body Green's function when Gorkov's equation is solved self-consistently. The end result is a tractable, accurate and gently scaling *ab initio* scheme applicable to full isotopic chains in the medium-mass region.

I. INTRODUCTION

In the last decade nuclear structure theory has been characterized by remarkable developments in *ab initio* calculations beyond the lightest isotopes. Different approaches like coupled cluster (CC) [1–3], Dyson self-consistent Green's functions (SCGF) [4–6] and in-medium similarity renormalization group (IM-SRG) [7, 8] are nowadays able to successfully describe the properties of nuclei in the region $A \sim 15 - 50$ starting solely from the knowledge of the underlying two- and three-nucleon forces. Such methods, while differing in the way of solving the many-body Schrödinger equation, have proven capable of calculations with a similar degree of accuracy, e.g. for ground-state energies in the oxygen chain [1, 6, 8].

Compared to CC and IM-SRG, SCGF has the added advantage of providing insight into the the many-body dynamics since it explicitly processes information on the spectral distribution of nucleons and their in-medium behavior [9–11]. So far, applications of SCGF to finite nuclei have been typically limited to doubly closed-shell isotopes. In few cases superfluid systems have been addressed within the Nambu-Gorkov formalism by including quasiparticle-phonon couplings in the self-energy, either phenomenologically [12] or in the framework of nuclear field theory [13]. Recently, we have introduced a fully *ab initio* approach based on the Gorkov ansatz that extends the SCGF formalism to open-shell nuclei [14, 15]. Together with the latest advances at the level of nucleon interactions, such development paves the way for an *ab initio* description of full isotopic chains in the medium-/heavy-mass region in the near future.

A crucial issue for *ab initio* approaches concerns the ability of performing numerical calculations in increasingly large model spaces, with the aim of thoroughly checking the convergence and consequently accessing heavier systems. More in general, *ab initio* methods should aim at assessing all sources of theoretical uncertainties and eventually include theoretical error bands in their results. The intent of the present work is to discuss in details the implementation of Gorkov-Green's function techniques in finite nuclei and study the uncertainties associated with different observables. In particular errors coming from model space truncations and from the numerical algorithms used in solving Gorkov's equation are investigated. Other sources of error, including the uncertainties related to nuclear interactions and to many-body truncations have already been discussed in the literature [6, 8] and will be addressed thoroughly for Gorkov theory in future works.

A long-established problem with the self-consistent calculation of single-particle propagators in finite systems concerns the rapid increase of the number of poles that are generated at each iterative step. The fast growth is not surprising since, as one approaches the limit of exact self-energy, the Lehmann expressions for the one-body Green's functions (see Eqs. (3) and (12) in the following) develop a continuous cut along the real energy axis in correspondence of unbound states. In practical calculations, a truncation of the model space implies a discretization of the self-energy and self-bound systems can be accurately calculated by reducing the continuous cut to a tractable number of effective poles. Generally this has been done by either binning the self-energy poles along the energy axis or by employing Lanczos algorithms to project the energy denominators onto smaller Krylov spaces [16–21]. The latter approach is preferable since the original self-energy is retrieved in the limit of increasing Krylov basis. However, the above calculations relied on the further approximation of making the self-energy diagonal in

* vittorio.soma@physik.tu-darmstadt.de
† c.barbieri@surrey.ac.uk
‡ thomas.duguet@cea.fr

the one-body Hilbert space. Ref. [22] reported that this approximation leads to inaccuracies and that different pivots are necessary in order to correctly reproduce the off-diagonal features of the self-energy, leading to a block Lanczos algorithm. Other works have avoided Krylov projections and performed self-consistent calculations by manually selecting the most relevant poles of the propagator, and collecting the others into few effective poles. This has led to successful investigations [23, 24]. However, it implies *ad hoc* procedures that might hinder systematic estimations of the errors involved.

In our recent studies based on SCGF [6, 15, 25, 26] we have followed Ref. [22] and implemented modified Lanczos and Arnoldi algorithms to perform block reduction to Krylov spaces defined by multiple pivots. This approach guarantees convergence to the full original self-energy in the limit of increasing Krylov space and, hence, it is suitable for application in *ab initio* calculations. However, no account has been given so far of the performance and accuracy of this method in nuclear structure applications. One aim of the present work is to fill this gap.

The paper is organized as follows. In Sec. II the theory of Gorkov-Green's functions is briefly reviewed, with focus on the aspects inherent to the solution of Gorkov's equation. In Sec. III the numerical implementation of Gorkov's equation is discussed, with particular emphasis on the modified Lanczos algorithm employed in the diagonalization. A remainder of the relevant Lanczos formulae as well as details on the treatment of chemical potentials can be found in the Appendix. The performance of the Krylov projection is analyzed in Sec. IV. In Sec. V different degrees of self-consistency in the iterative solution of Gorkov's equations are compared. The dependence on the model space is then investigated in Sec. VI, followed by final remarks in Sec. VII.

II. GORKOV-GREEN'S FUNCTION THEORY

A. Gorkov's equation

Given the intrinsic Hamiltonian

$$H_{\rm int} \equiv T + V - T_{CM} \ , \tag{1}$$

Gorkov-SCGF theory targets the ground state $|\Psi_0\rangle$ of the grand-canonical-like potential $\Omega \equiv H_{\rm int} - \mu_p \hat{Z} - \mu_n \hat{N}$, having the correct average number of protons, $Z = \langle\Psi_0|\hat{Z}|\Psi_0\rangle$, and neutrons, $N = \langle\Psi_0|\hat{N}|\Psi_0\rangle$. Here, μ_p (μ_n) is the proton (neutron) chemical potential and $\hat{Z}$ ($\hat{N}$) the proton- (neutron-)number operator.

The complete one-body dynamics with respect to the state $|\Psi_0\rangle$ is embodied in a set of four Green's functions known as Gorkov propagators [27][1]

$$\mathbf{G}(\omega) = \begin{pmatrix} G^{11}(\omega) & G^{12}(\omega) \\ G^{21}(\omega) & G^{22}(\omega) \end{pmatrix} . \tag{2}$$

Their matrix elements read in the Lehmann representation as

$$G^{11}_{ab}(\omega) = \sum_k \left\{ \frac{\mathcal{U}^k_a \mathcal{U}^{k*}_b}{\omega - \omega_k + {\rm i}\eta} + \frac{\bar{\mathcal{V}}^{k*}_a \bar{\mathcal{V}}^k_b}{\omega + \omega_k - {\rm i}\eta} \right\} , \tag{3a}$$

$$G^{12}_{ab}(\omega) = \sum_k \left\{ \frac{\mathcal{U}^k_a \mathcal{V}^{k*}_b}{\omega - \omega_k + {\rm i}\eta} + \frac{\bar{\mathcal{V}}^{k*}_a \bar{\mathcal{U}}^k_b}{\omega + \omega_k - {\rm i}\eta} \right\} , \tag{3b}$$

$$G^{21}_{ab}(\omega) = \sum_k \left\{ \frac{\mathcal{V}^k_a \mathcal{U}^{k*}_b}{\omega - \omega_k + {\rm i}\eta} + \frac{\bar{\mathcal{U}}^{k*}_a \bar{\mathcal{V}}^k_b}{\omega + \omega_k - {\rm i}\eta} \right\} , \tag{3c}$$

$$G^{22}_{ab}(\omega) = \sum_k \left\{ \frac{\mathcal{V}^k_a \mathcal{V}^{k*}_b}{\omega - \omega_k + {\rm i}\eta} + \frac{\bar{\mathcal{U}}^{k*}_a \bar{\mathcal{U}}^k_b}{\omega + \omega_k - {\rm i}\eta} \right\} . \tag{3d}$$

The poles of the propagators are given by $\omega_k \equiv \Omega_k - \Omega_0$, where the index k refers to normalized eigenstates of Ω that fulfill

$$\Omega\,|\Psi_k\rangle = \Omega_k\,|\Psi_k\rangle \, . \tag{4}$$

The residue of $\mathbf{G}(\omega)$ associated with pole ω_k relates to the probability amplitudes $\mathcal{U}^k$ ($\mathcal{V}^k$) to reach state $|\Psi_k\rangle$ by adding (removing) a nucleon to (from) $|\Psi_0\rangle$ on a single-particle state[2].

The one-body propagators of Eq. (3) are solutions of the Gorkov's equation of motion

$$\left.\begin{pmatrix} T + \Sigma^{11}(\omega) - \mu_k & \Sigma^{12}(\omega) \\ \Sigma^{21}(\omega) & -T + \Sigma^{22}(\omega) + \mu_k \end{pmatrix}\right|_{\omega_k} \begin{pmatrix} \mathcal{U}^k \\ \mathcal{V}^k \end{pmatrix} = \omega_k \begin{pmatrix} \mathcal{U}^k \\ \mathcal{V}^k \end{pmatrix} , \tag{5}$$

whose output is the set of vectors $(\mathcal{U}^k, \mathcal{V}^k)$ and energies ω_k. The chemical potential $\mu_k = \mu_p$ or μ_n depending on the particular charge quantum number carried by the pole k. Eq. (5) reads as a one-body eigenvalue problem in which the normal [$\Sigma^{11}(\omega)$ and $\Sigma^{22}(\omega)$] and anomalous [$\Sigma^{12}(\omega)$ and $\Sigma^{21}(\omega)$] irreducible self-energies act as *energy-dependent* potentials. Eventually, the total binding energy of the A-body system is computed via the Koltun-Galitskii sum rule [28]:

$$E_0^{\rm A} = \frac{1}{4\pi i} \int_{C\uparrow} d\omega\, {\rm Tr}_{\mathcal{H}_1} \left[G^{11}(\omega) \left[T + (\mu + \omega) \right] \right] , \tag{6}$$

which is exact for the case of two-body Hamiltonians.

---

[1] Two-dimensional matrices in Gorkov space are denoted in boldface throughout the paper. Non-boldface quantities are used for vectors and matrices defined on the one-body Hilbert space $\mathcal{H}_1$. The matrix elements of the lattes are denoted by latin letter subscripts $\{a, b, \ldots\}$, which label the single particle basis of $\mathcal{H}_1$.

[2] The component of vector $\mathcal{U}^k$ associated with a single-particle state a is denoted by $\mathcal{U}^k_a$. Correspondingly, the component associated with the time-reversed state $\bar{a}$ (up to a phase η_a) is denoted by $\bar{\mathcal{U}}^k_a$ [14].

Separation energies between the A-body ground state and eigenstates of $A \pm 1$ systems are related to the poles ω_k through

THOMAS: this equations was originally written in terms of 'A' and I have changed it to $\hat{N}$ and $\hat{Z}$ separated, for consistency with the discussion below Eq. (1). I am not sure it is right though: please check it!

$$E_k^{\pm} \equiv \mu_k \pm \omega_k = \pm\left[\langle\Psi_k|H_{\rm int}|\Psi_k\rangle - \langle\Psi_0|H_{\rm int}|\Psi_0\rangle\right] \mp\mu_k\left[\langle\Psi_k|\hat{Z}+\hat{N}|\Psi_k\rangle - (\mathrm{A}\pm 1)\right] , \quad (7)$$

where last term takes care of the error associated with the difference between the average number of particles in state $|\Psi_k\rangle$ and the targeted particle number $\mathrm{A} \pm 1$. Spectroscopic factors associated with the *direct* addition and removal of a nucleon are defined as

$$SF_k^{+} \equiv \mathrm{Tr}_{\mathcal{H}_1}\left[\mathcal{U}^k(\mathcal{U}^k)^\dagger\right] \quad \text{and} \quad SF_k^{-} \equiv \mathrm{Tr}_{\mathcal{H}_1}\left[\mathcal{V}^{k\,*}(\mathcal{V}^k)^T\right] . \quad (8)$$

In open-shell nuclei, the odd-even staggering of nuclear masses is a fingerprint of pairing correlations and offers, through finite odd-even mass difference formulae, the possibility to extract the pairing gap. The most commonly used [29] three-point-mass difference formula $\Delta_n^{(3)}(\mathrm{A})$ equates the pairing gap with the Fermi gap in the one-nucleon addition/removal spectra $E_k^{\pm}$, e.g. $\Delta_n^{(3)}(\mathrm{A}) \equiv (-1)^{\mathrm{A}}[E_0^+ - E_0^-]/2$. One-body observables such as mass or charge radii can be easily computed from $G^{11}(\omega)$ [14]. Moreover, effective single-particle energies (ESPE) introduced by Baranger as centroids $e_a^{\rm cent}$ of one-nucleon addition and removal spectra $E_k^{\pm}$ can be naturally computed in the present context [14, 30]. The normal self-energy $\Sigma^{11}(\omega)$ appearing in Eq. (5) is also identified with the microscopic nucleon-nucleus optical potential [26, 31], allowing for the computation of scattering states [32].

B. Self-energy expansion

The solution of the eigenvalue problem in Eq. (5) yields the complete set of $\{\mathcal{U}^k, \mathcal{V}^k, \omega_k\}$ from which one can fully reconstruct the Gorkov propagators. This requires the knowledge of the self-energy, which can always be written as the sum of a static (that is, energy independent) and a dynamic term:

$$\mathbf{\Sigma}(\omega) = \mathbf{\Sigma}^{(\infty)} + \mathbf{\Sigma}^{(dyn)}(\omega) . \quad (9)$$

The four static self-energies read

$$\Sigma_{ab}^{11\,(\infty)} = +\sum_{cd} V_{acbd}\,\rho_{dc} \equiv +\Lambda_{ab} = +\Lambda_{ab}^\dagger \quad (10a)$$

$$\Sigma_{ab}^{22\,(\infty)} = -\sum_{cd} V_{\bar{b}d\bar{a}c}\,\rho_{cd}^* = -\Lambda_{\bar{a}\bar{b}}^* , \quad (10b)$$

$$\Sigma_{ab}^{12\,(\infty)} = \frac{1}{2}\sum_{cd} V_{a\bar{b}c\bar{d}}\,\tilde{\rho}_{cd} \equiv +\tilde{h}_{ab} , \quad (10c)$$

$$\Sigma_{ab}^{21\,(\infty)} = \frac{1}{2}\sum_{cd} V_{b\bar{a}c\bar{d}}^*\,\tilde{\rho}_{cd}^* = +\tilde{h}_{ab}^\dagger , \quad (10d)$$

where V_{acbd} represent antisymmetrized matrix elements of the two-body interaction of Eq. (1) and ρ_{ab} and $\tilde{\rho}_{ab}$ are respectively the normal and anomalous density matrices

$$\rho_{ab} \equiv \langle\Psi_0|a_b^\dagger a_a|\Psi_0\rangle = \sum_k \bar{\mathcal{V}}_b^k\,\bar{\mathcal{V}}_a^{k*} , \quad (11a)$$

$$\tilde{\rho}_{ab} \equiv \langle\Psi_0|\bar{a}_b a_a|\Psi_0\rangle = \sum_k \bar{\mathcal{U}}_b^k\,\bar{\mathcal{V}}_a^{k*} . \quad (11b)$$

Note that Eqs. (10) are formally at first order in V_{acbd} and represent the Hartree-Fock and Bogoliubov diagrams. However, they are expressed in terms of the spectroscopic amplitudes of the exact (fully dressed) propagators. Thus, they implicitly resum all static higher order diagrams in perturbation theory. Eqs. (10) are also exact and complete for a two-body Hamiltonian. In the presence of three- or higher many-body interactions, they remain unchanged but acquire further contributions due to additional interaction reducible diagram [33].

If only first-order contribution to the self-energy are retained, Eqs. (5), (10) and (11) reduce to an *ab initio* Hartree-Fock-Bogoliubov (HFB) problem. At second and higher orders, the self-energy acquires energy dependent contributions to $\mathbf{\Sigma}^{(dyn)}(\omega)$ and the solution of Eq. (5) complicates. The dynamical part of the self-energy can be expressed through its Lehmann representation as follows

$$\Sigma_{ab}^{11\,(dyn)}(\omega) = \sum_\kappa \left\{ \frac{\mathcal{C}_a^\kappa\,(\mathcal{C}_b^\kappa)^*}{\omega - E_\kappa + \mathrm{i}\eta} + \frac{(\bar{\mathcal{D}}_a^\kappa)^*\,\bar{\mathcal{D}}_b^\kappa}{\omega + E_\kappa - \mathrm{i}\eta} \right\} , \quad (12a)$$

$$\Sigma_{ab}^{12\,(dyn)}(\omega) = \sum_\kappa \left\{ \frac{\mathcal{C}_a^\kappa\,(\mathcal{D}_b^\kappa)^*}{\omega - E_\kappa + \mathrm{i}\eta} + \frac{(\bar{\mathcal{D}}_a^\kappa)^*\,\bar{\mathcal{C}}_b^\kappa}{\omega + E_\kappa - \mathrm{i}\eta} \right\} , \quad (12b)$$

$$\Sigma_{ab}^{21\,(dyn)}(\omega) = \sum_\kappa \left\{ \frac{\mathcal{D}_a^\kappa\,(\mathcal{C}_b^\kappa)^*}{\omega - E_\kappa + \mathrm{i}\eta} + \frac{(\bar{\mathcal{C}}_a^\kappa)^*\,\bar{\mathcal{D}}_b^\kappa}{\omega + E_\kappa - \mathrm{i}\eta} \right\} , \quad (12c)$$

$$\Sigma_{ab}^{22\,(dyn)}(\omega) = \sum_\kappa \left\{ \frac{\mathcal{D}_a^\kappa\,(\mathcal{D}_b^\kappa)^*}{\omega - E_\kappa + \mathrm{i}\eta} + \frac{(\bar{\mathcal{C}}_a^\kappa)^*\,\bar{\mathcal{C}}_b^\kappa}{\omega + E_\kappa - \mathrm{i}\eta} \right\} , \quad (12d)$$

where $\mathcal{C}$ and $\mathcal{D}$ account for couplings of single quasiparticle excitations to configurations involving $2n+1$ quasiparticles, with $n \geq 1$, and E_κ labels the corresponding energies. The structure of Eqs. (12) is the same as for the exact self-energy and does not change if additional

many-body interactions enter the Hamiltonian. Up to this point no approximation has been made, if the exact self-energy is employed for (10) and (12) then the Gorkov's Eq. (5) is equivalent to solving the exact A-body Schrödinger equation.

In actual calculations, a truncation in the expansion of $\mathbf{\Sigma}(\omega)$ has to be adopted to approximate the coupling amplitudes ($\mathcal{C}^\kappa$, $\mathcal{D}^\kappa$) and their poles E_κ. In the present work first- and second-order self-energy contributions are considered in the solution of Gorkov's equations. By summing all eight second-order skeleton diagrams in terms of correlated propagators, one obtains an approximation for $\mathbf{\Sigma}^{(dyn)}(\omega)$ with the same form of Eqs. (12) where the label κ runs over all possible three-quasiparticles (3QP) excitations $\kappa = \{k_1, k_2, k_3\}$. The corresponding poles are then [14]

$$E_\kappa = E_{k_1k_2k_3} \equiv \omega_{k_1} + \omega_{k_2} + \omega_{k_3} \tag{13}$$

and the total coupling amplitude read

$$\mathcal{C}_a^{k_1k_2k_3} \equiv \frac{1}{\sqrt{6}}\left[\mathcal{M}_a^{k_1k_2k_3} + \mathcal{M}_a^{k_2k_3k_1} + \mathcal{M}_a^{k_3k_1k_2}\right], \tag{14a}$$

$$\mathcal{D}_a^{k_1k_2k_3} \equiv \frac{1}{\sqrt{6}}\left[\mathcal{N}_a^{k_1k_2k_3} + \mathcal{N}_a^{k_2k_3k_1} + \mathcal{N}_a^{k_3k_1k_2}\right], \tag{14b}$$

where

$$\mathcal{M}_a^{k_1k_2k_3} \equiv \sum_{ijk} V_{akij}\,\mathcal{U}_i^{k_1}\mathcal{U}_j^{k_2}\bar{\mathcal{V}}_k^{k_3}\,, \tag{15a}$$

and

$$\mathcal{N}_a^{k_1k_2k_3} \equiv \sum_{ijk} V_{akij}\,\mathcal{V}_i^{k_1}\mathcal{V}_j^{k_2}\bar{\mathcal{U}}_k^{k_3}\,. \tag{15b}$$

In the above formulation, both $\mathbf{\Sigma}^{(\infty)}(\omega)$ and $\mathbf{\Sigma}^{(dyn)}(\omega)$ depend on the spectroscopic amplitudes ($\mathcal{U}^k$,$\mathcal{V}^k$) and poles ω_k. This implies an iterative diagonalization of Gorkov's equation to achieve of self-consistency solutions.

C. Energy-independent form of the Gorkov's equation

Using the explicit energy dependence of the Lehmann representation, one can derive an alternative formulation of Gorkov's equation. Considering the second-order truncation of the self-energy expansion described above, one introduces the two additional amplitudes $\mathcal{W}$ and $\mathcal{Z}$ that describe the admixtures of 3QP configurations

$$(\omega_k - E_{k_1k_2k_3})\,\mathcal{W}_k^{k_1k_2k_3} \equiv \sum_a \left[(\mathcal{C}_a^{k_1k_2k_3})^*\,\mathcal{U}_a^k + (\mathcal{D}_a^{k_1k_2k_3})^*\,\mathcal{V}_a^k\right]\,, \tag{16a}$$

$$(\omega_k + E_{k_1k_2k_3})\,\mathcal{Z}_k^{k_1k_2k_3} \equiv \sum_a \left[\bar{\mathcal{D}}_a^{k_1k_2k_3}\,\mathcal{U}_a^k + \bar{\mathcal{C}}_a^{k_1k_2k_3}\,\mathcal{V}_a^k\right]\,, \tag{16b}$$

and rewrites Eq. (5) as

$$\omega_k\,\mathcal{U}_a^k = \sum_b \Big[(T_{ab} - \mu\,\delta_{ab} + \Lambda_{ab})\,\mathcal{U}_b^k + \tilde{h}_{ab}\,\mathcal{V}_b^k\Big] + \sum_{k_1k_2k_3}\Big[\mathcal{C}_a^{k_1k_2k_3}\,\mathcal{W}_k^{k_1k_2k_3} + (\bar{\mathcal{D}}_a^{k_1k_2k_3})^*\,\mathcal{Z}_k^{k_1k_2k_3}\Big]\,, \tag{17a}$$

$$\omega_k\,\mathcal{V}_a^k = \sum_b \Big[\tilde{h}_{ab}^\dagger\,\mathcal{U}_b^k - (T_{ab} - \mu\,\delta_{ab} + \Lambda_{\bar{a}\bar{b}}^*)\,\mathcal{V}_b^k\Big] + \sum_{k_1k_2k_3}\Big[\mathcal{D}_a^{k_1k_2k_3}\,\mathcal{W}_k^{k_1k_2k_3} + (\bar{\mathcal{C}}_a^{k_1k_2k_3})^*\,\mathcal{Z}_k^{k_1k_2k_3}\Big]\,. \tag{17b}$$

The four relations above provide a set of coupled equations for unknowns $\mathcal{U}$, $\mathcal{V}$, $\mathcal{W}$ and $\mathcal{Z}$ that can be recast in a matrix form

$$\omega_k \begin{pmatrix} \mathcal{U} \\ \mathcal{V} \\ \mathcal{W} \\ \mathcal{Z} \end{pmatrix}_k = \begin{pmatrix} h & \tilde{h} & \mathcal{C} & \bar{\mathcal{D}}^* \\ \tilde{h}^\dagger & -\bar{h}^* & \mathcal{D} & \bar{\mathcal{C}}^* \\ \mathcal{C}^\dagger & \mathcal{D}^\dagger & E & 0 \\ \bar{\mathcal{D}}^T & \bar{\mathcal{C}}^T & 0 & -E \end{pmatrix} \begin{pmatrix} \mathcal{U} \\ \mathcal{V} \\ \mathcal{W} \\ \mathcal{Z} \end{pmatrix}_k \equiv \Xi \begin{pmatrix} \mathcal{U} \\ \mathcal{V} \\ \mathcal{W} \\ \mathcal{Z} \end{pmatrix}_k\,, \tag{18}$$

where $h \equiv T - \mu + \Lambda$ and $E \equiv \mathrm{diag}\{E_\kappa\}$. The derivation of an energy-independent matrix Ξ can be generalized to higher-order truncations of self-energy as long as these can be expressed through the Lehmann representation (12).

III. NUMERICAL ALGORITHM

Exactly the same solutions are associated with Gorkov's equations in the form (5) or (18). For numerical implementations, however, the treatment of an energy-dependent eigenvalue equation might not be particularly

desirable. Attempts of solving directly the Eq. (5) have revealed problematic due to the energy denominators in $\mathbf{\Sigma}(\omega)$ that impliy drastic variations of the self-energy near its poles [34]. Even with very fine meshes in energy, this issue can still severely limit the resolution of the calculations [35]. Alternatively, each pole can be searched for individually [23, 36, 37]. But this involves a lengthy numerical procedure that does not guarantee obtaining all solutions of Eq. (5). In other words, a sizeable fraction of the spectral strength could be neglected. Working with Eq. (18), on the other hand, avoids the danger of divergences and automatically guarantees to extract all poles at once. The price to pay is a severe growth in the dimension of Gorkov's matrix, with consequent limitations on its diagonalization and high requirements in memory storage. Nevertheless, this eventually results in a gain of more than an order of magnitude in computational time with respect to solving directly for the poles of Eq. (5). As discussed in the following, the large dimensions of Ξ do not preclude convergence in model spaces that are large enough for modern *ab initio* nuclear structure calculations.

A. Self-consistency and dimensionality

Gorkov's matrix depends on the eigenvalues ω_k and amplitudes ($\mathcal{U}^k$,$\mathcal{V}^k$), which implies that the solution must be searched for iteratively. To see how the energy-independent form, Eq. (18), involves a drastic increase of the dimensionality of the problem at each iteration, let us separate the matrix Ξ as follows

$$\Xi = \left(\begin{array}{cc|cc} h & \tilde{h} & \mathcal{C} & \bar{\mathcal{D}}^* \\ \tilde{h}^\dagger & -\bar{h}^* & \mathcal{D} & \bar{\mathcal{C}}^* \\ \hline \mathcal{C}^\dagger & \mathcal{D}^\dagger & E & 0 \\ \bar{\mathcal{D}}^T & \bar{\mathcal{C}}^T & 0 & -E \end{array}\right) \equiv \left(\begin{array}{c|c} \Xi^{(1)} & \Xi^{(2)} \\ \hline \Xi^{(2)\,\dagger} & \mathcal{E} \end{array}\right) . \tag{19}$$

The number of states in the single-particle basis, N_b, defines the dimension of the first-order block $\Xi^{(1)}$ (see Fig. 1). Each of the four sub-blocks in $\Xi^{(1)}$ is $N_b \times N_b$, for a total of $2N_b \times 2N_b$ matrix elements. The matrix E is diagonal for second-order self-energies and its elements are all possible combinations of three energies $\{\omega_{k_1}, \omega_{k_2}, \omega_{k_3}\}$. Typically, a (mean-field) reference state is chosen as starting point so that only unperturbed quasiparticle states are present at the first iteration. In this situation, the number of quasiparticle states equals the dimension of the basis N_b and the number of poles in Eq. (12) is

$$N_s \approx \left(\begin{array}{c} N_b \\ 3 \end{array}\right) \approx \frac{N_b^3}{6} . \tag{20}$$

Since $N_b \ll (N_b)^3$ it follows that $\dim(\Xi) = N_{tot} \times N_{tot} \propto N_b^3/3 \times N_b^3/3$. In most cases, one can exploit spherical symmetry to split Gorkov's equations into uncoupled partial waves which equivalent to have a reduced effective number basis states to N_b^{eft} ≈10-20. However, N_b of order of a few hundreds are typically needed in order to achieve convergence for the most general cases. Thus, the full diagonalization of Gorkov's matrix for large model spaces may become unfeasible with current computational resources, even for the first iteration.

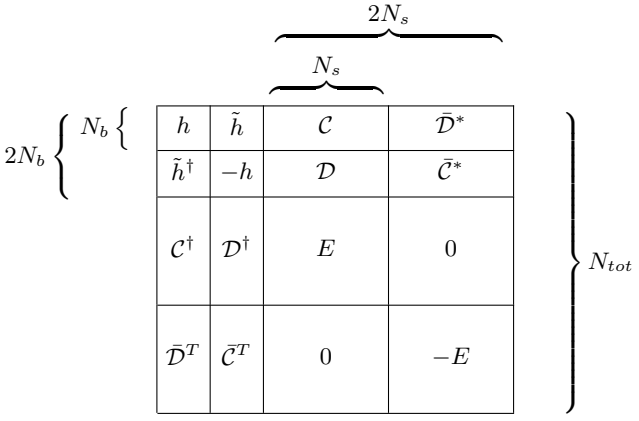

FIG. 1. Dimension scheme for the Gorkov matrix Ξ.

After Ξ is diagonalized, a number ≈ $(N_b)^3/6$ of new quasiparticle states appear, which can be seen as new fragments carrying a fraction of the single-particle strength. Those are new poles in the one-body propagators. In the second iteration, the possible combinations of three single-particle energies have then increased, resulting in $N_s \approx N_b^9/216/6$, which leads to $\dim(\Xi) \propto N_b^9/1000 \times N_b^9/1000$. In the n-th iteration the matrix Ξ will have expended to dimensions of the order of $N_b^{3^n} \times N_b^{3^n}$. Such a growth clearly prevents the exact treatment of all quasiparticle poles in an actual (self-consistent) calculation, where one has to keep $\dim(\Xi)$ below a threshold that is computationally tractable.

B. Krylov projection

In the present work we follow Ref. [22] and project the energy denominators of $\mathbf{\Sigma}^{(dyn)}(\omega)$ to a smaller Krylov subspace. This allows to contain the dimensional growth of the Gorkov matrix and to develop a sustainable computational procedure.

In terms of the Gorkov matrix of Eq. (18), we generate a set of pivot vectors p^i with elements

$$p^i_\kappa = \sum_a \mathcal{C}^\kappa_a U^i_a \; + \; \sum_a \mathcal{D}^\kappa_a V^i_a \, , \tag{21}$$

where (U^i, V^i) are linearly independent vectors in the HFB one-body Hilbert space. In general, one needs a pivot for each single-particle orbit in the model space to properly converge all the off-diagonal elements of Eqs.(12) [22]. Up to $2N_b$ starting pivots are then used to generate a Krylov subspace $\mathcal{K}$ associated with the submatrix E in Eq. (18). Our particular implementation uses

a Lanczos-type algorithm that starts from one pivot at a time and iterates it N_ℓ times, independently of the others. Each time iterations are started with a new pivot, p^i, this is first orthogonalised with respect to the basis vectors already generated. This is equivalent to a block Lanczos reduction based on a slightly modified set of pivots $\{p^{i\prime}\}$. Eventually, the dimension of the Krylov space is the number of *total* Lanczos iterations, $N_L = \dim(\mathcal{K}) = N_\ell \times N_{pivots}$. Full details of the algorithm are given in Appendix A.

The block $\mathcal{E}$ in Eq. (19) thus reduces to a matrix of lower dimensions

$$\mathcal{E} \longrightarrow \mathcal{E}' = \begin{pmatrix} \mathcal{L}^\dagger E \mathcal{L} & \\ & -\mathcal{L}^\dagger E \mathcal{L} \end{pmatrix} , \tag{22}$$

where $\mathcal{L}$ is the collection of vectors generated by the Lanczos procedure. The two off-diagonal blocks $\Xi^{(2)}$ and $\Xi^{(2)\,\dagger}$ are transformed accordingly:

$$\Xi^{(2)} \longrightarrow \Xi'^{(2)} = \Xi^{(2)} \begin{pmatrix} \mathcal{L} \\ \mathcal{L} \end{pmatrix} , \tag{23a}$$

$$\Xi^{(2)\,\dagger} \longrightarrow \Xi'^{(2)\,\dagger} = \begin{pmatrix} \mathcal{L}^\dagger & \mathcal{L}^\dagger \end{pmatrix} \Xi^{(2)\,\dagger} . \tag{23b}$$

These projected blocks are inserted in the original Gorkov matrix

$$\Xi \longrightarrow \Xi' = \left(\begin{array}{c|c} \Xi^{(1)} & \Xi'^{(2)} \\ \hline \Xi'^{(2)\,\dagger} & \mathcal{E}' \end{array}\right) , \tag{24}$$

whose dimensions are now $\dim(\Xi') = 2N_b + 2N_L$. The Gorkov-Krylov matrix Ξ' is finally (fully) diagonalized with standard diagonalization routines. In terms of Lehmann representation, Eq. (12), the Krylov projected quantities results in approximating the exact self-energy as

$$\Sigma^{(2)} = \mathcal{C} \frac{1}{\mathbb{1}\omega - E} \mathcal{C}^\dagger \;\; \longrightarrow \;\; \Sigma'^{(2)} = \mathcal{C}\,\mathcal{L} \frac{1}{\mathbb{1}\omega - \mathcal{L}^\dagger E \mathcal{L}} \mathcal{L}^\dagger \mathcal{C}^\dagger , \tag{25}$$

where only the first term in Eq. (12a) has been considered schematically. The other terms follow accordingly.

The number of Lanczos iterations N_L controls the dimension of the matrix Ξ' that undergoes diagonalization. For a sufficiently large number of iterations $\dim(\mathcal{K}) \longrightarrow \dim(E)$ and the exact results is recovered.

Notice that the technique outlined here differs in spirit from the standard use of Lanczos or Arnoldi algorithms in large-scale shell-model diagonalizations. In fact, while these methods aim at excellent estimates of the first lower eigenvalues of a large-matrix, in Green's function calculations one is rather interested in reproducing most of the key features of the spectral distribution. The Krylov subspace projection of a matrix ensures a fast convergence at the extremes of its eigenvalue spectrum. Thus, it is important that the Lanczos algorithm is applied separately to both sub-blocks E and $-E$ of Eq. (19), which are mirrored across the Fermi energy. In this way the quasiparticle spectrum near the Fermi surface is recovered accurately upon diagonalizing Eq. (24). The other important property of Krylov subspace techniques is that the first $2N_\ell$ moments of each pivot are conserved during the projection. This ensures that the overall distribution of single-particle strength converges quickly, which is important for achieving good estimates for all observables after a relatively small number of Lanczos iterations.

C. Calculation scheme

As mentioned above, a typical Gorgov Green's function calculation involves an iterative procedure that leads to a self-consistent solution for the four Gorkov propagators. In practice, the following steps are performed:

1. A reference single-particle propagator is used as an initial set of $\{\mathcal{U}^k, \mathcal{V}^k, \omega_k\}$ and $\{\mu_p, \mu_n\}$. This is normally generated by solving the first order HFB problem.

2. Second order self-energies are computed through Eqs. (13) to (15).

3. The self-energy is projected to a suitable Krylov subspace acceding to Eqs. (22) and (23).

4. The energy-independent self-energies that enter $\Xi^{(1)}$ are computed by means of Eqs. (10).

5. The matrix Ξ' [Eq. (24)] is constructed and diagonalized.

6. The chemical potentials μ_p and μ_n are adjusted to yield the correct number of protons and neutrons of the targeted nucleus according to Eq. (B2). This involves several re-diagonalizations of the matrix Ξ' with adjustments of μ_p and μ_n alone.

7. The solution (i.e. a new set of $\{\mathcal{U}^k, \mathcal{V}^k, \omega_k\}$ and $\{\mu_p, \mu_n\}$) constitutes the new single-particle propagator that is used as input for the successive iterations. The calculations is re-started from point 2 for full self-consistency (or point 4 for the partial "sc0" scheme discussed below).

The above procedure is repeated until convergence is achieved. This is usually assessed by looking at the variation of chemical potentials or total binding energy, which can be computed at each iteration by means of the Koltun-Galitskii sum rule (6). In the present work the convergence criterium is set by variations in the total energy that are smaller than 1 keV. As discussed in the next section, such value is smaller than the systematic error on binding energies.

Repeating the points 2–6 above leads to the fully self-consistent ("sc") implementation of Gorkov-Green's functions. In this case the converged results are completely independent of the reference states adopted at point 1. A computationally cheaper alternative—referred to as "sc0" in the following—consists in iterating only points 4–6. In other words, self-consistency is limited to

the energy independent part of the self-energy [$\Xi^{(1)}$ in Eq. (19)] while the matrix elements of the second order $\mathbf{\Sigma}^{(dyn)}(\omega)$ are computed once and afterwards frozen. In actual calculations it is common to employ HFB propagators as reference states for generating the second order skeleton diagrams. Thus, a substantial portion self-energy insertion diagrams (beyond second order) are effectively recovered. However, the partial self-consistency in the sc0 approach already retains the most important features since it implicitly generates all energy independent diagrams above first order through the dressing of propagators in Eqs. (10) and (11). As opposed to perturbation theory, the key, self-consistent character of Green's function methods guarantees the resummation of self-energy insertions to all orders and makes the method intrinsically non-perturbative and iterative. Since the present self-energy is complete at second order, both sc0 and sc generate all diagrams for $\mathbf{\Sigma}^{(\infty)}$ are retained up to third order and all those for $\mathbf{\Sigma}^{(dyn)}(\omega)$ up to and second order. In both cases, the self-consistency in $\mathbf{\Sigma}^{(\infty)}$ automatically includes all-order resummations of several diagrams beyond third order.

The two schemes will be compared in details in Sec. V, where in particular it will be shown that the sc0 degree of self-consistency is capable of grasping most of the correlations introduced by second-order self-energies.

D. Numerical scaling

An important issue for *ab initio* approaches concerns the possibility of performing numerical calculations with increasingly large model spaces, so that it is possible to control their convergence and access heavier systems. Thus, we analyze in some detail the numerical scaling properties of Gorkov-Green's function calculations. Provided that a full diagonalization of the unprojected Gorkov's matrix is computationally too expensive, we will directly consider the cost of calculations that use the Lanczos algorithm.

The benefit of the Krylov projection is the reduction of dimensionality of the Gorkov eigenvalue problem. At each iteration, after projecting and before the diagonalization (step 5 in Sec. III C), the size of Gorkov's matrix is determined by the total number of Lanczos vectors, N_L. In particular, the projected 3QP matrix, $E' \equiv \mathcal{L}^\dagger E \mathcal{L}$, has the dimension of the Krylov subspace, such that the dimension of the eigenvalue problem for Ξ' is

$$N'_{tot} = 2\,N_b + 2\,N_L\,. \tag{26}$$

In general, $N_L \ll N_s$ which results in a tremendous reduction of dimensionality. Not only $\dim(E') \ll \dim(E)$ but $N_L = 2\,N_b \times N_\ell$ is independent of the number to poles in the iterated propagator. Thus, $\dim(E')$ remains small due to the Krylov projections at each iteration, allowing for self-consistent calculations even for large bases.

Before comparing of the overall costs for the sc0 and sc calculations, we look at the scaling of separate steps of the algorithm in Sec. III C. In general, the three main steps are the calculation of the Gorkov matrix, its Krylov reduction, and its diagonalization. Only the last step is iterated in a sc0 calculation. These have different scaling behaviors when varying model and Krylov spaces:

1. While the matrix E is trivial at second order, $\Xi^{(2)}$ has $2N_b \times 2N_s$ elements to be computed. For the first iteration and the sc0 scheme, $N_s \approx N_b^3/6$ and the elements of $\Xi^{(2)}$ are simply the interaction matrix elements expressed in the reference (HFB) basis. For successive iterations, $N_s \propto N_L^3$ while $\Xi^{(2)}$ requires projecting the interaction on the Gorkov orbitals [see Eqs. (15)]. This requires number of operations $\propto N_b \times N_s \times N_b^3$. Hence, calculating the Gorkov matrix scales as follows:
   - For the first iteration and sc0: $\propto N_b^4$;
   - For successive iterations in sc: $\propto N_b^7\,N_\ell^3$.
2. The Lanczos algorithm iteratively generates N_L basis vectors of dimension N_s. Within this procedure, the most time consuming part is again the projection of the coupling amplitudes to obtain $\Xi'^{(2)}$ [see Eqs. (23)], which is a matrix multiplication requiring $2N_b \times N_s \times N_L$ steps. Hence, The Krylov projection scales as:
   - For the first iteration and sc0: $\propto N_b^5\,N_\ell$;
   - For successive iterations in sc: $\propto N_b^5\,N_\ell^4$.
3. The diagonalization of the Gorkov matrix always scales like $(N'_{tot})^3 \propto N_b^3\,N_\ell^3$, for large values of N_ℓ.

All considerations made so far are valid for a general choice of the single-particle basis $\{a_a^\dagger\}$, such as the case of an m-scheme calculation, and represent a worst case scenario. Our actual implementation considers nuclei that are assumed to be in a $J^\Pi = 0^+$ state, for which the Gorkov equations naturally decouple into partial waves of definite charge, angular momentum and parity, $\alpha \equiv (q, j, \pi)$ [14]. In general, the basis of a given partial wave, α, will have a dimension N_b^α that corresponds to the number of its principal levels included in the model space. The dimension of the associated Krylov space, $N_L^\alpha = 2\,N_b^\alpha\,N_\ell$, will vary with α accordingly. This changes the above stated scaling properties in a non trivial way. The present calculations use a spherical harmonic oscillator basis with all orbits included up to a maximum shell $N_{\max} = \max\{2n_\alpha + \ell_\alpha\}$. This basis has $N_b^\alpha \leq N_{\max}/2$ but its sclalings gain an extra power in N_b^α because the same calculations are performed separately for all partial waves: more precisely, $\sum_\alpha (N_b^\alpha)^\gamma \propto (N_{\max})^{\gamma+1}$ for large $N_{\max}$. Note, however, that the relevant quantity for the m-scheme case its the total number of all possible single particle orbits, $N_b^{tot} = \sum_\alpha N_b^\alpha \propto (N_{\max})^2$, which grows faster than $N_{\max}$. Hence, decoupling all partial waves results in a high gain in terms of computational times. In addition, for a fixed $N_{\max}$, the dimensions of the Lanczos

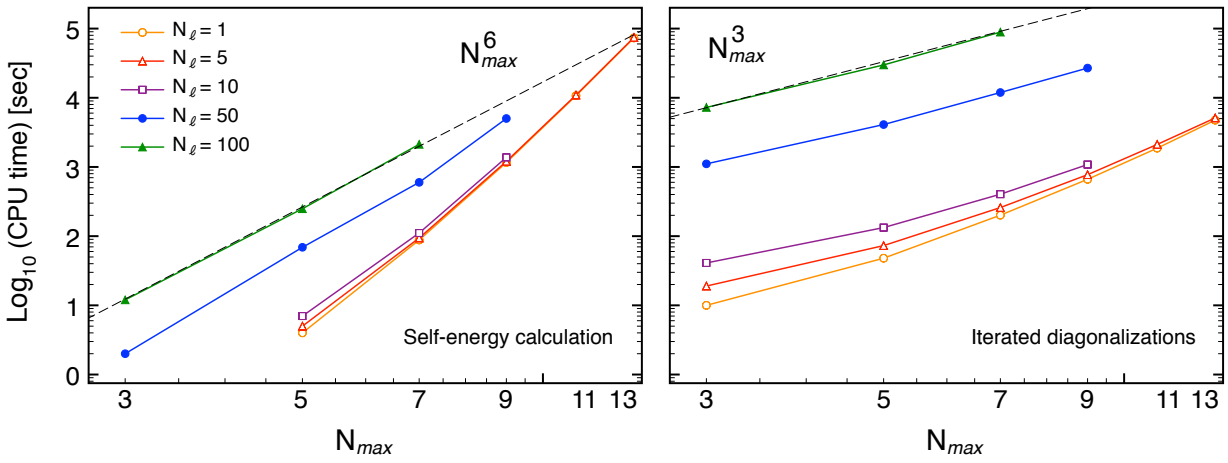

FIG. 2. CPU time spent in parts of a typical sc0 calculation as a function of $N_{\max}$ and for different values of N_ℓ. Left panel: time needed to calculate the self-energies for all partial waves $\{\alpha\}$ and projecting them to Krylov subspaces (points 1 and 2 of Sec. III D). Right panel: time required for diagonalising the Gorkov matrices of all partial wave over 100 sc0 iterations (point 3 of Sec. III D). Dashed lines show scaling of the type $(N_{\max})^\gamma$, with γ =6 and 3.

vectors, N_s^α, are no longer proportional to $(N_b^\alpha)^3$ but it will have a bell shape with increasing angular momentum, j_α, that is due to combinatorics in coupling angular moments. This also also affects the considerations at points 1 and 2 above and results in a more gentle scaling.

Since the actual scaling in computer time depends non trivially on the model space chosen, we tested for our algorithm directly in actual calculations. The results are shown in Fig. 2 for a series of sc0 runs on a single processor. The left panel shows the time required for generating the Krylov-reduced Gorkov matrix (steps 1 and 2 above) for different model space sizes and different N_ℓ. At large values of N_ℓ the computation time is dominated by the Lanczos procedure and scales as $\approx N_{\max}^6$, as expected. The calculation of the second order self-energy (step 1) is relevant only for very few Lancsoz iterations (when step 2 is negligible). Hoerver, it increases more rapidly with respect to $N_{\max}$, indicating that for large model spaces an improvement of our algorithm for step 1 might be in order. The right panel shows the time required for 100 diagonalizations of the Gorkov matrix (steps 4-6 of Sec. III C). This is representative to the typical number of sc0 iterations needed in actual calculations to converge both the propagator and the chemical potentials. As expected, the actual step of diagonalising Eq. (24) becomes dominant for a large N_ℓ and scales as $\approx N_{\max}^3$. Both panels of Fig. 2 reflect the actual computing time of a typical sc0 calculation and indicate that resources are evenly split between the Krylov subspace projections and sc0 iterations to reach self-consistency.

From the above scaling properties, it is clear that the full sc scheme is sensibly more expensive than the corresponding sc0. This is shown in Fig. 3 for typical Gorkov calculations in different model spaces and Krylov projections, as determined by the number of Lanczos iterations per pivot N_ℓ. Evidently, the sc implementation is much more costly than the sc0. In fact, even when projected to small Krylov spaces, the time required for running the sc scheme can easily become prohibitive for practical purposes. On the other hand, as discussed in Sec. V, the sc0 scheme already grasps all the relevant physics leading to accurate results (see also Refs. [6, 15]) and can be applied to even larger model spaces that are, e.g., necessary to handle SRG-unevolved realistic interactions. The sc0 is therefore an optimal choice for practical calculations.

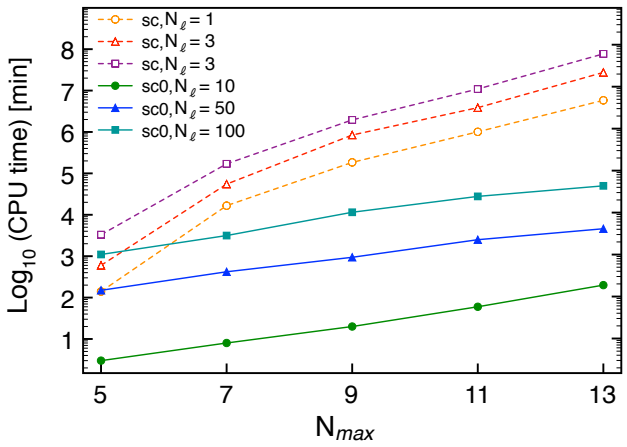

FIG. 3. Typical CPU time requirements (in minutes) for 100 iterations in the sc and sc0 self-consistency schemes. Times are shown for different Krylov subspaces (characterized by the same number of Lanczos iterations per pivot, N_ℓ) as a function of the model space dimensions.

IV. PERFORMANCE OF KRYLOV PROJECTION

As already mentioned, we assume the nuclei under study to be in a $J^\Pi = 0^+$ state and expand the Gorkov GFs propagators in a spherical harmonic oscillator basis with quantum number $a = (n, q, j, m, \pi) \equiv (n, \alpha, m)$, where n and m respectively label the principal quantum number and the projection of the third component of angular momentum. This allows us to simplify the working equations into a block diagonal form that separates all the possible partial waves α. Unless otherwise stated, the two-body potential employed here is a next-to-next-to-next-to-leading-order (N^3LO) 2N chiral interaction [38, 39] (Λ_χ =500 MeV) complemented by the Coulomb force. The resulting isospin-symmetry breaking interaction is then softened using free-space similarity renormalization group (SRG) techniques [40] down to a momentum scale of $\lambda = 2.0$ fm^{-1}.

Before discussing numerical results for the Gorkov propagators and associated quantities, we investigate the technical steps involved in the Krylov projection to ensure that these do not introduce uncontrolled errors. First, we check the convergence of the Lanczos algorithm employed with respect to the different choices of pivot vectors. Second, we investigate the actual dependence of binding energies and spectral quantities on the size of the Krylov subspace. This allows us to make statements on the best compromise between high accuracy and an affordable computational cost.

N_ℓ	N_p	$N_L/N_L^{crit,*}$	E$_{(\nu s_{1/2})}$ [MeV]
1	4	4	-2.286045527516
5	4	20	-2.285370055029
10	4	40	-2.285503728538
50	4	200	-2.285578135207
100	4	400	-2.285580911804
150	4	600	-2.285580911686
200	4	800	-2.285580911686
297	4	1111*	-2.285580911686
300	3	1121*	-2.285580911686
400	3	1113*	-2.285558373049
800	2	1103*	-2.285504651650
1000	2	1029*	-2.285580911687
1188	1	1029*	-2.215766990937
Exact diagonalization:			-2.285580911686

TABLE I. Contribution to the total binding energy from the neutron $s_{1/2}$ partial wave in ^{12}C, for different numbers pivot used (N_p) and number of iterations per pivot (N_ℓ). Asterisks (*) indicate a truncation of the Lanczos iterations at N_L^{crit} due to sudden loss of orthogonality. Otherwise, a total number N_L=$N_p \times N_\ell$ vectors is generated. The dimension of the full 3QP space is $N_s^{\nu s_{1/2}}$=1188.

N_ℓ	N_p	N_L	E$_{(\nu s_{1/2})}$ [MeV]
600	1	600	-2.109743018672
300	2	600	-2.268918978484
200	3	600	-2.279490387096
150	4	600	-2.285580911686
Exact diagonalization:			-2.285580911686

TABLE II. Same as Tab. II but for a fixed total number of Lanczos vectors and varying the number of linearly independent pivots.

A. Choice of Lanczos pivots

In exact arithmetic, the Lanczos algorithm generates basis vectors that are all orthogonal to each other, until the full original space is spanned. On a computer, the finite precision of the machine will at some point spoil such orthogonality, resulting in a set of linearly dependent vectors. This can be usually corrected, e.g., by means of selective orthogonalization techniques [41]. In the following we take instead a pedantic approach and orthogonalize, at the end of each Lanczos iteration, the new Lanczos vector with respect to all previous ones. This procedure is increasingly costly in the limit of large N_L, but it is doable and the provedes safest option for actual calculations where one is interested in relatively small Krylov spaces. An additional mechanism causing the sudden loss of orthogonality is related to the convergence of the eigenvalues of the Krylov-projected matrix, known as Ritz (eigen)values, to machine precision. This however happens only for extremely large spaces that approach the dimension of the original space [Eq. (27) below] and does not affect in practice our Gorkov calculations. Nevertheless, we still check for sudden losses orthogonality between successive Lancozs vectors[3]. If such a case occurs we truncate the projection right before, at a corresponding N_L^{crit} number of iterations.

A first basic test concerns the limit

$$N_L = \dim(E') \longrightarrow \dim(E) \tag{27}$$

[see also Eq. (A2)], where the Krylov subspace coincides with the initial one and the exact result must be recovered. To this extent, we calculate the partial contribution of one specific channel to the biding energy of ^{12}C, Eq. 6, in a small model space where projections can be compared to an exact diagonalization. Tabs. I and II give the contributions to the Koltun-Galitskii sum rule for a neutron with $j^\pi = 1/2^+$ (α=$\nu s_{1/2}$) in small model space of 4 major oscillator shells ($N_{\max} = 3$) and for different numbers of iterations and pivots used. In this case $N_s^{\nu s_{1/2}}$=dim(E) = 1188, $N_b^{\nu s_{1/2}} = 2$ and the total dimension of the HFB space is dim($\Xi^{(1)}$) = 4. Thus, only up

[3] Following Ref. [41], two vectors $\mathbf{v}$ and $\mathbf{w}$ are considered orthogonal if $\mathbf{v} \cdot \mathbf{w} < \sqrt{\epsilon_m}$, where ϵ_m is the machine precision. In the case of the present calculations $\epsilon_m = 1.11 \cdot 10^{-16}$.

to 4 Lanczos pivots can be generated from linearly independent vectors in the HFB space, Eq. 21. As long as the number of iterations per pivot, N_ℓ, is small enough to allow for all the $2N_b^{\nu s_{1/2}}$ pivots to be used, the Krylov-projected energy converges to the exact value in the limit (27). Tab. I shows that 600 iterations, corresponding to half of the original 3QP configurations, is enough to recover the exact diagonalization to thirteen significant digits. Even for N_ℓ=50, results are converged to less than 10 eV. However, when N_ℓ increases a smaller number of pivots is exploited before the full space is saturated. The accuracy gradually worsens as the number of pivots actually used is decreased, although results close to exact one are still found for two pivots only. In principle, even one single pivot should be sufficient to eventually recover the exact diagonalization in the limit (27). In practice, however, no more than a few % accuracy is achieved before the loss of orthogonality kicks in. Conversely, by adding just a few extra iterations of a second pivot the calculated energy collapses close to the exact result. The dependence on the number of pivots used is shown in Tab. II for a fixed dimension of the final Krylov space. This shows that the best possible accuracy is obtained if all possible linearly independent pivots are iterated. We further found that including all pivots is important to quickly converge all the off diagonal matrix elements of the self-energies, Eqs. (12), in accordance with the finding of Ref. [22]. This dependence on the number of pivots relates to having enough degrees of freedom to be able to span the original HFB space and is particularly important when resolvent operators are involved in the projection, as it is the case in Green's function theory.

In general, any set of linearly independent vectors in the HFB Hilbert space can be used to generate the pivot for the Krylov space through Eq.(21). In our calculations we find that the optimal choice is given by the HFB basis, which was employed in the above tests. Vectors in the harmonic oscillator basis as well as random basis vectors lead to worse convergence in all cases considered. Various calculations with different orbitals, nuclei, interactions or model spaces confirmed the above considerations. Given this, $2N_b$ pivots generated from the HFB basis are used throughout the following.

B. N_ℓ dependence

When going to the large model spaces necessary to converge calculations with realistic nuclear interactions, the currently available computational resources set severe technical limits on the dimensions of the matrix Ξ that are tractable numerically. A crucial issue concerns how large should the Krylov subspace be in order to achieve a satisfactory accuracy in the solution of the Gorkov equation. In particular, we examine the dependence of the results on the number of Lanczos iterations per pivot, N_ℓ. We do this by first looking at the dependence on single partial waves (as already considered in Tab. I). Then,

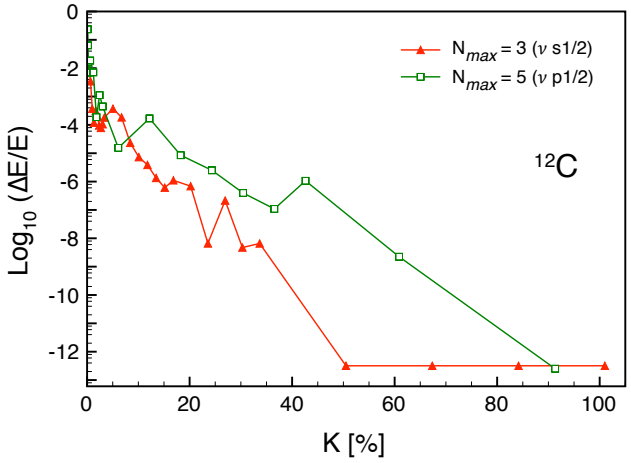

FIG. 4. Relative error in the Koltun-Galitskii sum rule contribution from a single orbital α in ^{12}C as a function of K^α. Results refer to one diagonalization, for two separate partial waves and different model spaces.

we investigate the convergence for the cases of just one Gorkov iteration (involving all waves at once) and for complete self-consistent sc0 calculations.

For a given model space, the dimensions of both the 3QP space, N_s, and the single particle basis, N_b, will vary with the partial wave $\alpha = (q, j, \pi)$. Consequently, for each α block, a fixed number of Lanczos iterations N_ℓ generates a Krylov-projected matrix, E', that span different portions of the initial space. To quantify this, we introduce

$$K^\alpha \equiv 100 * \frac{\dim(E'^\alpha)}{\dim(E^\alpha)} = \frac{100 * N_\ell * 2N_b^\alpha}{\dim(E^\alpha)}\,, \qquad (28)$$

measuring the fraction of the initial 3QP configuration space retained by the Krylov projection. This should give a rough estimate of the percentage of the full 3QP degrees of freedom that enter the diagonalization of the Gorkov matrix.

Figure 4 shows the convergence of the contribution to the Koltun-Galitskii sum rule, Eq (6), of two separate partial waves in ^{12}C as a function of K^α and for model spaces with $N_{\max} = 3$ and $N_{\max} = 5$. This gives a representative way of how the error of partial contribution decreases by orders of magnitude with increasing N_ℓ. In particular relatively small values of K^α are sufficient to achieve precisions of the order of the keV in both cases. After this initial transient the error follow a exponentially decreasing trend. The $\nu s_{1/2}$ wave reaches the exact results up to machine precision when half of the 3QP space is projected to the Krylov subspace, as already pointed out in Table I. For the larger model space the convergence to the exact result is eventually slower but, importantly, the transient of the first few iterations remains.

As discussed before, the use of one (global) value for N_ℓ implies different degrees of approximation (K^α) for

$N_{\max}$	$\alpha_{\rm tot}$	$\sum_\alpha \dim(E^\alpha)$	$\sum_\alpha 2N_b^\alpha$	$K'(N_\ell = 100)[\%]$
3	7	12 226	20	16.358
4	9	57 029	30	5.260
5	11	411 968	42	1.019
7	15	3 265 512	72	0.220
9	19	16 808 456	110	0.065
11	23	65 305 228	156	0.023
13	27	208 096 960	210	0.010

TABLE III. Values entering Eq. (29) for various model spaces. The sum over α is limited to neutrons only (including protons would require a factor 2 in columns 2, 3 and 4 and cancels out in K'). As an example, K' values for $N_\ell = 100$ are displayed in the last column.

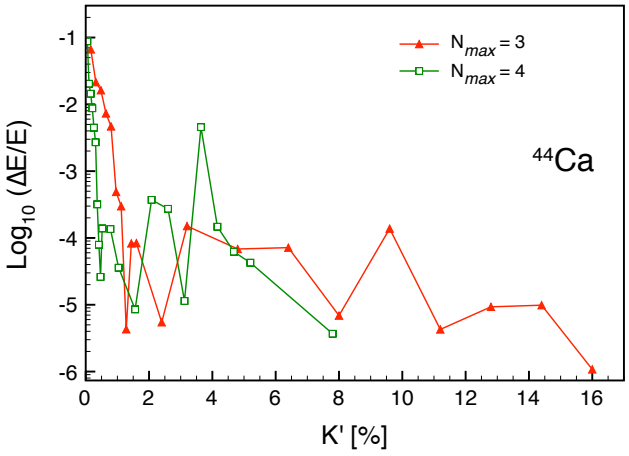

FIG. 5. Relative error in the total binding energy of ^{44}Ca after one second-order iteration (with μ adjustment), given as a function of K' for two different model spaces.

each partial contribution to the total energy. In general $N_L^\alpha \propto N_b^\alpha$ so that partial waves with lower angular momentum will be better reproduced on average, since for given $N_{\max}$ truncation of the harmonic oscillator space the number of orbits N_b^α decreases with increasing j_α. This is desirable because low angular momentum waves correspond to the most occupied orbits and give stronger contributions to the total binding energy, through Eq. (6). To analyze the combined behavior of all contributions it is convenient to consider the overall fraction of 3QP degrees of freedom retained,

$$K' \equiv 100 * \frac{\sum_\alpha \dim(E'^\alpha)}{\sum_\alpha \dim(E^\alpha)} = \frac{100 * N_\ell * \sum_\alpha 2N_b^\alpha}{\sum_\alpha \dim(E^\alpha)}\,, \quad (29)$$

where α runs over all partial waves. The values entering Eq. (29) are displayed in Table III for different $N_{\max}$. Note that for a fixed N_ℓ the fraction K' becomes progressively very small with increasing size of the model space. However, the total number of degrees of configurations still grows with N_b^α, and asymptotically as $(N_{\max})^2$.

Fig. 5 demonstrates the accuracy of the total binding energy as a function of K', when all possible partial

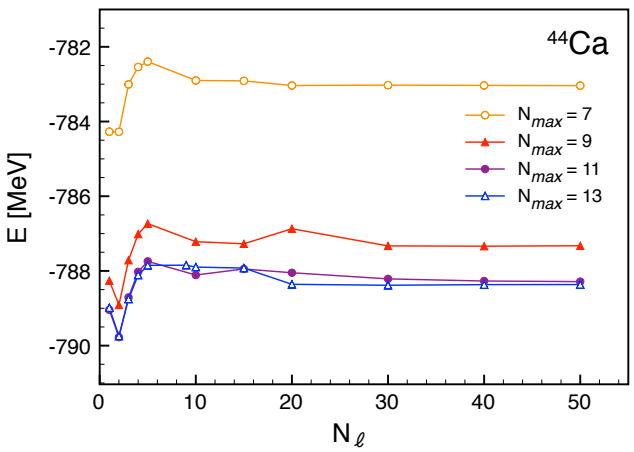

FIG. 6. Converged (sc0) total binding energy of ^{44}Ca for different model spaces as a function of N_ℓ.

waves are accounted for. The ^{44}Ca isotope in considered here. The Gorkov matrix is diagonalised only once but with the chemical potentials already adjusted to yield the correct number of particles. Relative errors are given with respect to a complete (unprojected) diagonalization. Errors in both $N_{\max} = 3$ and $N_{\max} = 4$ models spaces are comparable for $K' > 1\%$ and eventually decrease in a similar fashion as in Fig. 4. On the other hand, convergence to few keV is reached for smaller values of K' in the larger model space.

Actual calculations will differ from the above cases for the fact that several diagonalizations have to be repeated iteratively to reach self-consistency and that very large model spaces must be employed. In Fig. 6 converged sc0 energies are displayed for different model model spaces as a function of N_ℓ. One notices that all cases show a similar dependence on N_ℓ: a dip, a steep rise after $N_\ell = 2$ and a smooth decay towards an asymptotic value. This behaviour is rather independent of $N_{\max}$ and indicates that N_ℓ is a much better parameter than K' for gauging the convergence of the Krylov projections. On the other hand, small fluctuations can still happen for $N_\ell > 10$, especially for the larger models spaces, and suggest that somewhat larger values of N_ℓ might be needed to reach the desired accuracy as $N_{\max}$ increases. In general, this behaviour is in accordance with the above observations that, when enlarging the model space, smaller K' fractions are sufficient to reach a few keV accuracy. Arguably, binding energies are well reproduced once one includes a minimal number of degrees of freedom that is sufficient to resolve the system's wave function (or propagator). This is well controlled by N_ℓ and happens no matter how big is the fraction of the 3QP configurations that are left out. The Krylov projection is a very efficient way to select such key degrees of freedom since it specifically preserves the moments of the 3QP matrix E. The trend observed in Figs. 4 and 5 suggest that K' might instead control the exponential convergence to the

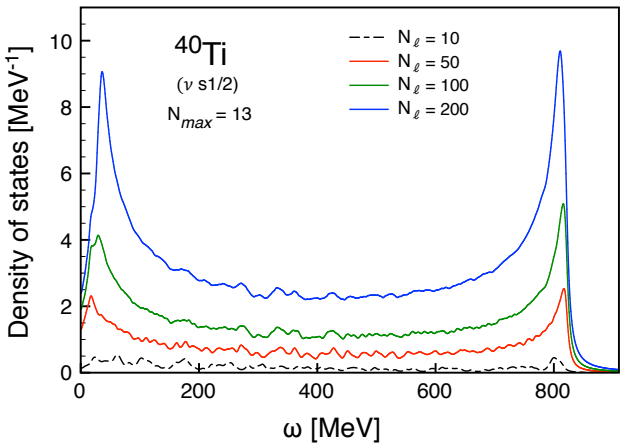

FIG. 7. Density of neutron $1/2^+$ states in ^{40}Ti for different Krylov projections. Due to the symmetry of Gorkov's equation, the distribution is symmetric around $\omega = 0$. The distribution, discretized in the calculation, is convoluted with Lorentzian curves of 5 MeV width for display purposes.

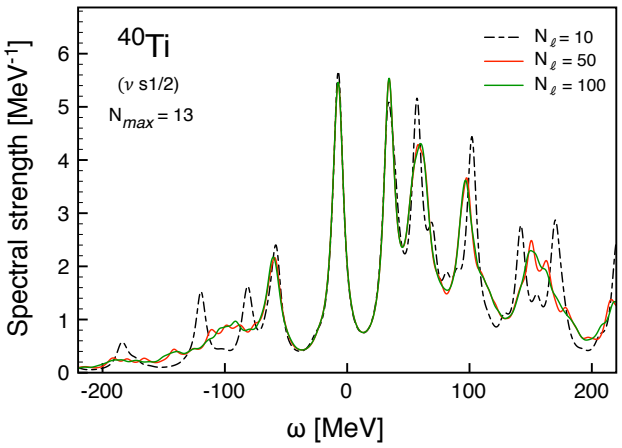

FIG. 8. One-neutron addition and removal spectral strength distribution in the $1/2^+$ channel in ^{40}Ti. The same cases of Fig. 7 are shown. The distribution, discretized in the calculation, is convoluted with Lorentzian curves of 5 MeV width for display purposes.

exact diagonalization. This is the plateau of Fig. 6, after the initial transient that reconstructs the most important features of the propagator.

A proper estimate of the error introduced by the projection into a Krylov subspace should eventually be based on varying the N_ℓ parameter, and it can differ for various model space sizes and calculated isotopes. From Fig. 6 one sees that the energies reach a plateau in the N_ℓ dependence for $N_\ell > 30$, rather independently of the model space. By looking at the sc0 values obtained here, we estimate that the Lanczos procedure up to N_ℓ=50 introduces accuracies of roughly 200-300 keV for the largest model space considered ($N_{\max} = 13$).

It is also instructive to look at convergence of spectroscopic quantities with respect to the Krylov projections. To this purpose, the case of the doubly open-shell nucleus ^{40}Ti is considered in a model space of 14 major shells. In Fig. 7 the density of (quasiparticle) neutron $1/2^+$ states is displayed as a function of their separation energy for increasing Lanczos iterations. The exactly calculated density of states (DOS) would have a bell shape due to the rise of the number of (physical) degrees of freedom which is eventually stopped by the truncation of the model space. From Tab. III, it is obvious that only a very small fraction of configurations cab be retained. Thus, as the dimension of the projected Gorkov matrix increases, only the density of states at the edges of the eigenvalue spectrum start converging, which is a typical feature of Krylov methods. Despite of the lack of degrees of freedom ad the center of the spectrum, the total spectral strength is shown to converge rather rapidly everywhere when increasing N_ℓ [42]. This is seen in Fig. 8, where the one-neutron addition and removal spectral strength distribution is computed for the same cases of Fig. 7. This is convoluted with Lorenzians of 5 MeV width, and

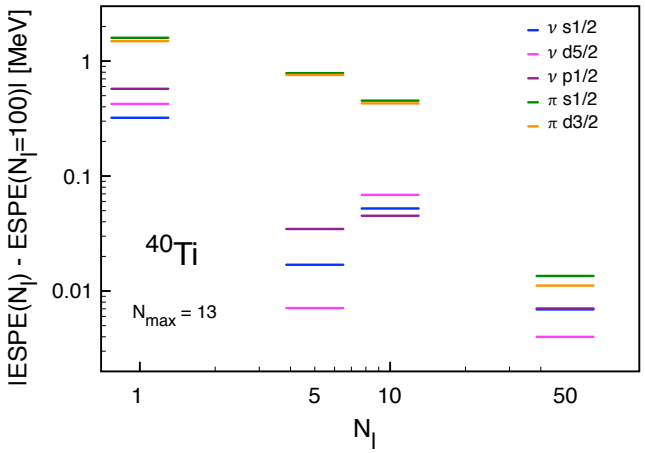

FIG. 9. Effective single-particle energies in ^{40}Ti, as a function of the Lanczos iterations N_ℓ, relative to the values computed with $N_\ell = 200$. Calculations are performed in an $N_{\max} = 13$ model space. Results are displayed for different neutron and proton orbitals.

the two $N_\ell = 100$ and $N_\ell = 200$ curves are substantially indistinguishable. We find that the strength distribution converges to a resolution of 10 MeV (5 MeV) for N_ℓ=50 ($N_\ell = 100$). Even for projections into relatively small Krylov spaces, the method conserves the overall features of the strength distribution, which guarantees the quick convergence of observables and spectroscopic quantities in general.

Fig. 9 also compares effective single-particle energies for various orbitals are at different Lanczos truncations N_ℓ. Results are given as deviation to the ESPE for the case $N_\ell = 200$ which is the most accurate truncation

used. Difference between $N_\ell = 50$ and $N_\ell = 200$ are already around 10 keV for all single-particle orbitals, and decrease to ?? keV for N_ℓ=100-200. This is also representative of the accuracy reached in calculations separation energy of dominating qp peaks. Similar results are obtained for other nuclei and different model spaces.

Summarizing, the Krylov projection is shown to be reliable in all the considered cases. The loss of orthogonality is well understood for small model spaces and never occurs in practice for large model spaces, where one is limited to a small number of Lanczos iterations. Both total binding energies and single-particle spectra are very well reproduced after relatively small values of N_ℓ, nearly independently of the original dimensions of Gorkov's matrix. This indicates that the Krylov-projection techniques employed here are a reliable and computationally affordable tool that can be extended to large model spaces. In view of these results, for a typical large-scale calculation a projection with $N_\ell = 50$ is expected to yield a sufficient degree of accuracy for most application to medium mass isotopes. In this case, a conservative estimate for the systematic error introduced by the projection is 500 keV on the converged total energy and 50 keV for what concerns one-nucleon separation energies and ESPEs. This can be improved by increasing N_ℓ.

V. SELF-CONSISTENCY SCHEMES

Section III C outlines two different self-consistent calculation schemes. The sc implementation corresponds to a fully self-consistent solution of Gorkov's equations. Instead, the sc0 scheme iterates self-consistently only the static part of Gorkov self-energies, $\mathbf{\Sigma}^{(\infty)}$. A priori, there is no guarantee that one of these two many-body truncations will give results systematically closer than the other to the exact binding energy. However, the sc approach is conceptually superior both because it includes more diagrams (at very high order) and because it guarantees that solutions will satisfy fundamental conservation laws. From the computational point of view the two approaches are very different (see Fig. 3). As discussed in Sec. III D, the heaviest part of a self-consistent iteration in the sc scheme is constituted by the computation of second-order self-energy matrix elements $\mathbf{C}$ and $\mathbf{D}$. This scales as $N_b^7 N_\ell^3$ after the first iteration, since a number $N_b + N_L$ of new poles have been generated, and it is much heavier than the corresponding sc0 case. Even with the most modern computational resources such a scaling puts severe limits on the model space and/or the accuracy (in terms of Krylov projection) that can be reached in actual calculations. The sc0 case, on the other hand, involves a much less demanding computational effort: second-order terms are computed only once in this scheme and for a propagator involving many N_b poles. Once this is done, the most costly part of a sc0 calculations is the diagonalization of the Krylov-projected Gorkov matrices in the various partial waves (step 3 in Sec. III D). We also

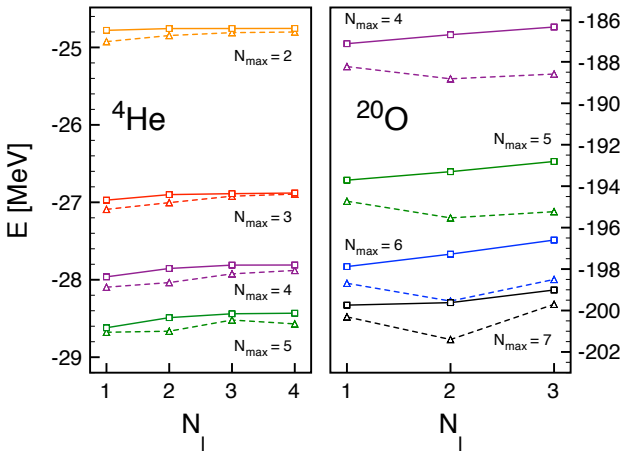

FIG. 10. Binding energy of ^{4}He (left) and ^{20}O (right) as a function of Lanczos iterations per pivot N_ℓ, for different model spaces. Dashed (solid) lines correspond to the sc (sc0) self-consistent scheme.

note that discrepancies between sc and sc0 are expected to be reduced once truncations of the Gorkov formalism beyond second order will be implemented.

The two self-consistency implementations are compared in Fig. 10 for ^{4}He and ^{20}O, using second order self-energies. Results for total binding energies are displayed for different model spaces and small Krylov subspace projections, for which full sc calculations were possible. For all the cases considered here, the two schemes yield results that differ at the level of 1%. This is about the same error estimated for many-body truncation in third- and higer-order SCGF approaches [6, 43]. Thus, Fig. 10 confirms the excellent performance of the partially self-consistent sc0 approach, making it the optimal compromise between high accuracy and an affordable computational cost.

VI. MODEL SPACE CONVERGENCE

The previous discussion has focused on the different technical steps that enable an efficient numerical solution of Gorkov's equation (18). In the present section, let us turn to the choice of the model space in Gorkov calculations. A crucial requirement for *ab initio* approaches is in fact the convergence with respect to the basis employed. For the harmonic oscillator model space considered here, this translates into the independence of the results on the oscillator spacing $\hbar\omega$ and number of major shells used $N_{\max} + 1$. Fig. 11 demonstrates the convergence of total energy of the open-shell ^{44}Ca. As $N_{\max}$ is increased, results become independent of $\hbar\omega$ and quickly converge to a fixed value. Calculations at first (second) order in the self-energy expansion vary by only 10 keV (30 keV) when going from $N_{\max} = 11$ to $N_{\max} = 13$, well below the systematic error introduced by the Krylov pro-

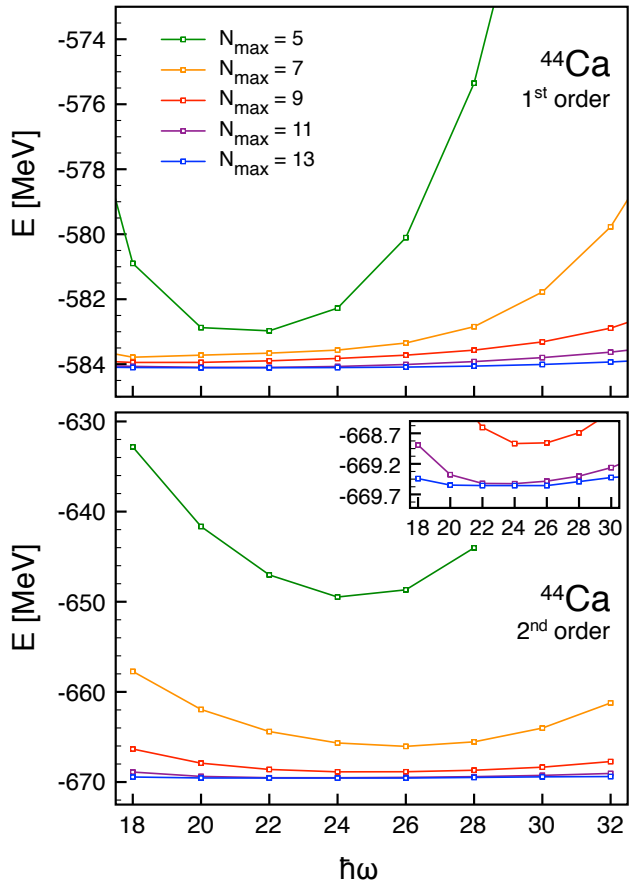

FIG. 11. Binding energies of ^{44}Ca from first-order (upper panel) and second-order (lower panel) Gorkov calculations as a function of the harmonic oscillator spacing $\hbar\omega$ and for increasing size $N_{\max}$ of the single-particle model space. The insert shows a zoom on the most converged results.

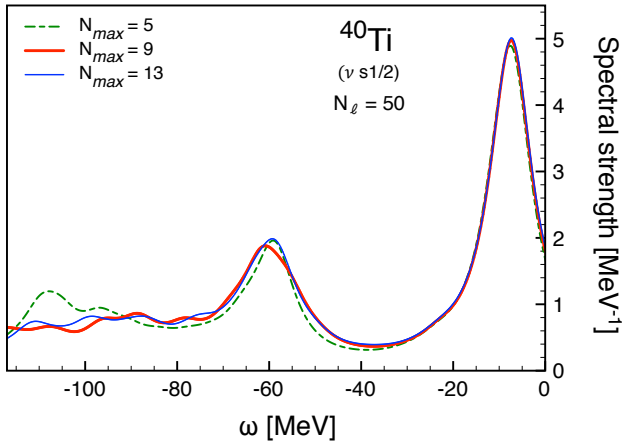

FIG. 12. One-neutron removal spectral strength distribution in the $1/2^+$ channel in ^{40}Ti as a function of the model space dimension $N_{\max}$. The distribution, discretized in the calculation, is convoluted with Lorentzian curves of 5 MeV width for display purposes.

jection. Similar convergence patterns have been found for closed shell calcium isotopes, as well as heavier systems such as ^{74}Ni [15]. Similar conclusions can be drawn for other quantities such as the spectral strength distribution. In Fig. 12, the one-neutron removal distribution, at energies below the Fermi level, is plotted for different values of $N_{\max}$. Details of the spectral distributions close to the Fermi surface are very well converged already at $N_{\max} = 9$. The distribution of Fig. 12 is convoluted with Lorentzians of 5 MeV, which demonstrates that model spaces of $N_{\max} = 11$ and $N_{\max} = 13$ are sufficient to converge the strength at very high (negative) energies to within this resolution.

For a given method and implementation, the convergence depends in general on the input NN (and 3N) interaction. In this sense, the robust behavior displayed in Fig. 11 confirms the softness of SRG-evolved potentials used in this work, for which 14 major shells are sufficient to ensure well converged calculations. Our present implementation leaves room for improvement of the algorithms and better parallelisation so that the method can be pushed to larger model spaces. This presents opportunities for either going to even heavier systems or employing interactions with a higher SRG cutoff. Both paths will be explored in forthcoming works.

VII. CONCLUSIONS

We have presented details of the numerical implementation of Gorkov-Green's function method for finite nuclear systems. This approach allows to extend the reach of first-principle calculations to several hundreds of open-shell nuclei in the medium-mass region that have been so far unaccessible. The complete Gorkov-Green's function formalism up to second order has been detailed in Ref. [14]. In this work, the numerical solution of these equations is discussed with particular attention to diagonalization, convergence and self-consistency issues. Presently we focus on an *ab initio* scheme whose input is a nucleon-nucleon N^{3}LO chiral interaction, SRG-evolved to $\lambda = 2.0$ fm^{-1}. Work to include three-nucleon forces is in progress and will be reported in a forthcoming publication (see also Ref. [6, 33]). The details and performance of the algorithm discussed in Secs. III and IV are however of general character, and will not be altered by the use of a stronger input NN interactions or the inclusion of three-body forces.

A distinctive feature of Green's function methods is the simultaneous generation of both the $A+1$ and $A-1$ spectral distributions, when computing the (ground-state) properties of the A-body system. Self-energy contributions beyond first order account for dynamical correlations and induce the fragmentation of the single-particle strength in such distributions. The self-consistent treat-

ment of the fragmented strength requires particular attention in handling the new poles that are generated at each iteration. Given the doubling of the effective degrees of freedom, due to the Bogoliubov ansatz, this is even more delicate when working in the Gorkov framework. We adopt a method to control the growth of poles in the single-particle propagator that makes use of Krylov projection techniques and it is a variant of methods already in use in Quantum Chemistry [22]. This is described in Sec. III, while Sec. IV presents specific details that are relevant to nuclear physics implementations. This procedure displays a favorable scaling behavior and can be executed to arbitrary accuracy, i.e. it recovers the exact result when the projection space coincides with the original one. In Sec. IV, we have studied the performance of our Krylov-based technique. We have shown that it is manageable from the numerical point of view, stable and benchmarked it against the exact result for small model spaces.

Two different self-consistent schemes have also been analyzed. With the currently available computational resources, a fully self-consistent implementation is out of reach for medium-mass nuclei. Nevertheless, the partially self-consistent sc0 scheme was seen to be already a satisfactory compromise as it leads to accurate results and it is also computationally feasible.

We have finally investigated the dependence of our results on the size of the harmonic oscillator model space, showing a very fast convergence of different observables when SRG-evolved interactions are employed.

From the technical point of view, this work demonstrates that Gorkov-Green's function calculations are a solid and viable candidate for the *ab initio* description of medium-mass open-shell nuclei. The method has proven to perform well both on semi-magic and doubly-magic systems up to the nickel isotopes [15, 25]. Together with the on-going implementation of three-nucleon interactions, the present work sets the basis for systematic calculations of full isotopic chains from an *ab initio* perspective.

ACKNOWLEDGMENTS

This work was supported by the United Kingdom Science and Technology Facilities Council (STFC) under Grants No. ST/I003363/1 and No.ST/J000051/1, by the DFG through Grant No. SFB 634, and by the Helmholtz Alliance Program, Contract No. HA216/EMMI. VS acknowledges support from Espace de Structure Nucléaire Théorique (ESNT) at CEA/Saclay. Calculations were performed using HPC resources from GENCI-CCRT (Grant No. 2012-050707) and the STFC DiRAC facility (Grant No.).

Appendix A: Krylov projection

The critical step that allows for Gorkov calculations in large configuration spaces is the projection of the 3QP configurations space into tractable Krylov subspace. Here, we present the details of the particular Lanczos-based algorithm presently employed in calculations of Gorkov- and Dyson-Green's functions [6, 15, 25, 26].

When solving Eq. (19), one needs to handle a matrix E of large dimensions $N_s \times N_s$. Let $\mathcal{H}_{LG}$ be the space spanned by the eigenvalues of E, with $\dim(\mathcal{H}_{LG}) = N_s$, and $\mathbf{p}$ a vector of dimension N_s (usually referred to as the pivot). The Krylov subspace of order r is the linear subspace of $\mathcal{H}_{LG}$ spanned by the images of $\mathbf{p}$ under the first r powers of E, i.e.

$$\mathcal{K}^{(r)} \equiv \text{span}\left\{\mathbf{p}, H\,\mathbf{p}, H^2\,\mathbf{p}, H^3\,\mathbf{p}, \ldots, H^{r-1}\,\mathbf{p}\right\} . \quad \text{(A1)}$$

Provided that E does not decouple in sub-blocks of separate symmetry, one has that

$$\mathcal{K}^{(N_s)} = \mathcal{H} . \quad \text{(A2)}$$

The Lanczos algorithm is a procedure that generates an orthonormal basis $\{\mathbf{v}_j;\, j = 1, 2, \ldots r\}$ of $\mathcal{K}^{(r)}$ in the case in which E is Hermitian. The basis vectors $\mathbf{v}_j$ are obtained through a recursive procedure that involves vector-matrix multiplications, as follows:

$$\begin{aligned}
\mathbf{v}_1 &\equiv \mathbf{p} && \text{(A3a)}\\
E\,\mathbf{v}_1 &\equiv e_{11}\,\mathbf{v}_1 + e_{21}\,\mathbf{v}_2 && \text{(A3b)}\\
E\,\mathbf{v}_2 &\equiv e_{12}\,\mathbf{v}_1 + e_{22}\,\mathbf{v}_2 + e_{32}\,\mathbf{v}_3 && \text{(A3c)}\\
&\cdots\\
E\,\mathbf{v}_{r-1} &\equiv e_{1(r-1)}\,\mathbf{v}_1 + \cdots + e_{r(r-1)}\,\mathbf{v}_r\ , && \text{(A3d)}
\end{aligned}$$

where at each step the newly generated vector $\mathbf{v}_j$ is further normalized to 1. Following the above construction one has

$$e_{ij} = (e_{ji})^* = \mathbf{v}_i^\dagger E\,\mathbf{v}_j = 0 \qquad \text{for } |i-j| \geq 2\,, \quad \text{(A4)}$$

such that the projection E' of the matrix E on $\mathcal{K}^{(r)}$ is tridiagonal.

A similar procedure is applied here to reduce response operators such as Eq. (25), where E is defined in a large configuration space $\mathcal{H}_{LG}$ and the matrix product $\mathcal{C}\mathcal{C}^\dagger$ is defined in a smaller space $\mathcal{H}_{SM}$. In this situation, it becomes necessary to exploit more than a single pivot vector to quickly converge all degrees of freedom in $\mathcal{H}_{SM}$. In our Gorkov calculations, $\mathcal{H}_{SM}$ is the HFB one-body Hilbert space, which has twice the dimension of the single-particle basis employed. Thus, we generate $n_p = 2N_b$ different vectors according to Eq. (21).

Let $\{\mathbf{p}^{(i)}; i = 1, \ldots n_p\}$ be a set of linearly independent vectors. The new Krylov space is generated by extending the definition of Eq. (A1) and the Lanczos procedure (A3) to the case of multiple pivots. Each vector

$\mathbf{p}^{(i)}$ is thus iterated a number of times r_i, so that the total dimension of the basis generated is

$$N_L = \sum_{i=1}^{n_p} r_i \ . \tag{A5}$$

In our algorithm the Lanczos iterations (A3) are performed in sequence for each starting vector $\mathbf{p}^{(i)}$. It if therefore important that, at the starting of each new set of iterations, the pivots are orthonormalized to the previously generated basis vectors.

The first pivot $\mathbf{p}_1$ is simply iterated r_1 times as follow:

$$\mathbf{v}_1^{(1)} \equiv \mathbf{p}^{(1)} \tag{A6a}$$
$$E\,\mathbf{v}_1^{(1)} \equiv e_{11}\,\mathbf{v}_1^{(1)} + e_{21}\,\mathbf{v}_2^{(1)} \tag{A6b}$$
$$\dots$$
$$E\,\mathbf{v}_{r_1}^{(1)} \equiv e_{(r_1-1)r_1}\,\mathbf{v}_{r_1-1}^{(1)} + e_{r_1 r_1}\,\mathbf{v}_{r_1}^{(1)} + \mathbf{u}^{(1)} \ . \tag{A6c}$$

Up to this point the projected matrix E' still maintains a tridiagonal structure and the vector $\mathbf{u}^{(1)}$ is orthogonal to the first r_1 basis vectors $\{\mathbf{v}_1^{(1)}, \dots \mathbf{v}_{r_1}^{(1)}\}$. As already mentioned, $\mathbf{p}_2$ has first to be orthogonalized with respect to the latters. Hence, one writes

$$\mathbf{p}^{(2)} \equiv \sum_{i=1}^{r_1} c_i^{(1)}\,\mathbf{v}_i^{(1)} + d^{(1)}\,\mathbf{v}_1^{(2)} \ , \tag{A7}$$

imposing $||\mathbf{v}_1^{(2)}|| = 1$, and takes $\mathbf{v}_1^{(2)}$ as the new pivot. Since $\mathbf{v}_1^{(2)}$ is orthogonal to all previous vectors, using the hermiticity of H and the tridiagonal form of Eqs. (A6) one can prove that

$$\mathbf{v}_i^{(1)\,\dagger} E\,\mathbf{v}_1^{(2)} = 0 \qquad \forall\, i = 1, \dots, r_1 - 1 \ , \tag{A8a}$$
$$\mathbf{v}_{r_1}^{(1)\,\dagger} E\,\mathbf{v}_1^{(2)} = \mathbf{u}^{(1)\dagger}\mathbf{v}_1^{(2)} = h_{r_1(r_1+1)} \ . \tag{A8b}$$

In general, each vector $\mathbf{p}^{(i)}$, with $i \geq 2$, will be orthonormalised to the previously generated portion of the basis according to

$$\mathbf{p}^{(i)} \equiv \sum_{j=1}^{i-1}\sum_{k=1}^{r_i} c_k^{(j)}\,\mathbf{v}_k^{(j)} + d^{(i)}\,\mathbf{v}_1^{(i)} \ , \tag{A9}$$

and the vector $||\mathbf{v}_1^{(i)}|| = 1$ is taken as the new pivot, which is iterated r_i times. If n_i is then number of basis vectors generated from all iterations before the i^{th} pivot,

$$n_i = \sum_{j=1}^{i-1} r_j \ , \tag{A10}$$

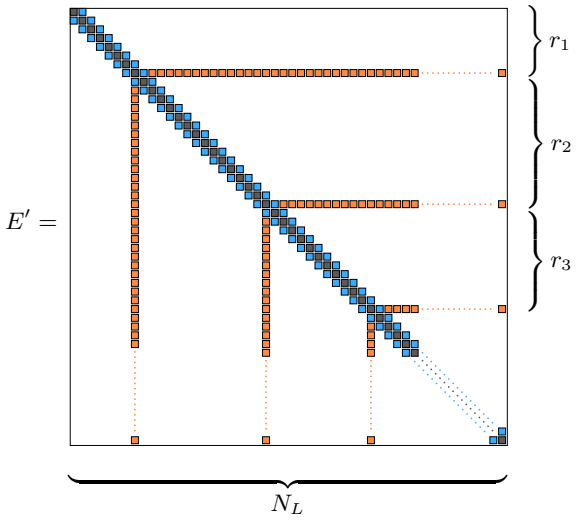

FIG. 13. Fishbone-like structure of the Lanczos reduced matrix E'.

the iteration of pivot $\mathbf{v}_1^{(i)}$ yelds

$$E\,\mathbf{v}_1^{(i)} \equiv \sum_{j=1}^{i-1} h_{n_j(n_i+1)}\,\mathbf{v}_{r_j}^{(j)} + h_{(n_i+1)(n_i+1)}\,\mathbf{v}_1^{(i)} + h_{(n_i+2)(n_i+1)}\,\mathbf{v}_2^{(i)} \tag{A11a}$$
$$E\,\mathbf{v}_2^{(i)} \equiv \sum_{j=1}^{i-1} h_{n_j(n_i+2)}\,\mathbf{v}_{r_j}^{(j)} + h_{(n_i+1)(n_i+2)}\,\mathbf{v}_1^{(i)} + h_{(n_i+2)(n_i+2)}\,\mathbf{v}_2^{(i)} + h_{(n_i+3)(n_i+2)}\,\mathbf{v}_3^{(i)} \tag{A11b}$$
$$\dots$$
$$H\,\mathbf{v}_{r_i}^{(i)} \equiv h \sum_{j=1}^{i-1} h_{n_j(n_i+r_i)}\,\mathbf{v}_{r_j}^{(j)} + h_{(n_i+r_i-1)(n_i+r_i)}\,\mathbf{v}_{r_i-1}^{(i)} + h_{(n_i+r_i)(n_i+r_i)}\,\mathbf{v}_{r_i}^{(i)} + \mathbf{u}^{(i)} \ , \tag{A11c}$$

where $\mathbf{u}^{(i)}$ is orthogonal to all previous vectors.

Relations analogous to Eqs. (A8) hold for every change to a new pivot, which connects the $\mathbf{v}_{r_i}^{(i)}$ vectors (at the end of each block of iterations) to the remaining basis vectors. It follows that the tridiagonal form of the projected matrix E' is maintained except for the rows and columns where pivots are changed, which are non-zero and give rise to the fishbone-like sparse matrix shown in Fig. 13.

Notice also that the resulting space is not directly generated by the $\mathbf{p}^{(i)}$ vectors of Eq. (21) since these are othogonalized before they are iterated. Hence, the actual Krylov space is the one associated with the pivots

$\{\mathbf{v}_1^{(i)}; i = 1, \ldots, n_p\}$ and it is defined as

$$\begin{aligned}\mathcal{K}^{(r)} \equiv \text{span}\Big\{ & \mathbf{v}_1^{(1)}, H\,\mathbf{v}_1^{(1)}, H^2\,\mathbf{v}_1^{(1)}, \ldots, H^{r_1-1}\,\mathbf{v}_1^{(1)}\,, \\ & \mathbf{v}_1^{(2)}, H\,\mathbf{v}_1^{(2)}, H^2\,\mathbf{v}_1^{(2)}, \ldots, H^{r_2-1}\,\mathbf{v}_1^{(2)}\,, \\ & \ldots \\ & \mathbf{v}_1^{(n_p)}, H\,\mathbf{v}_1^{(n_p)}, \ldots,\ H^{r_{n_p}-1}\,\mathbf{v}_1^{(n_p)} \Big\}\,. \end{aligned} \tag{A12}$$

In the present work we choose a fixed number of iterations, i.e. $r_i = N_\ell,\ \forall\, i = 1, \ldots n_p$, except for cases where a truncation of the Lanczos procedure required a lower number of iterations for the last pivot (bottom part of Tab. I).

Appendix B: Adjustment of chemical potentials

During the numerical solution of Gorkov's equation, at each iteration proton and neutron chemical potentials have to be adjusted in order to have, on average, the desired number of particles (see point 6 of the algorithm in Sec. III C). After the self-energies have been computed and Gorkov's matrix has been diagonalized, the average numbers of neutron and proton are evaluated through

$$N^{av} = \sum_a^{\text{neutrons}} \rho_{aa} = \sum_{a,k}^{\text{neutrons}} \left|\mathcal{V}_a^k\right|^2\,, \tag{B1a}$$

$$Z^{av} = \sum_a^{\text{protons}} \rho_{aa} = \sum_{a,k}^{\text{protons}} \left|\mathcal{V}_a^k\right|^2\,. \tag{B1b}$$

The resulting numbers are compared to the expected N and Z. The corresponding chemical potentials μ_N and μ_Z are then increased (decreased) if the computed number of particle is smaller (larger) than the required values according to

$$\mu_{N,Z}^{new} = \mu_{N,Z}^{old} + \Delta_{N,Z}^{\mu}\,, \tag{B2}$$

where

$$\Delta_N^{\mu} \equiv C_N^{\mu}\,\frac{N - N^{av}}{N}\,, \tag{B3a}$$

$$\Delta_Z^{\mu} \equiv C_Z^{\mu}\,\frac{Z - Z^{av}}{Z}\,. \tag{B3b}$$

The parameters $C_{N,Z}^{\mu}$ control the speed and pattern of convergence, and are typically of order of unity. As long as convergence is reached, the choice of $C_{N,Z}^{\mu}$ does not impact the final result.

Notice that subsequent adjustments of the chemical potentials may be necessary before the required precision of N^{av}, Z^{av} is achieved, implying that in practice the above procedure is repeated several times. However, one is not interested (at least in the first few iterations) in having extremely precise neutron and proton numbers as the self-consistency process will make the optimal chemical potentials vary until a sufficient degree of self-consistency is reached.

[1] G. Hagen, M. Hjorth-Jensen, G. Jansen, R. Machleidt, and T. Papenbrock, Phys. Rev. Lett. **108**, 242501 (2012).
[2] G. Hagen, M. Hjorth-Jensen, G. R. Jansen, R. Machleidt, and T. Papenbrock, Phys. Rev. Lett. **109**, 032502 (2012).
[3] S. Binder, J. Langhammer, A. Calci, P. Navrátil, and R. Roth, Phys. Rev. C **87**, 021303 (2013).
[4] C. Barbieri, Phys. Rev. Lett. **103**, 202502 (2009).
[5] C. Barbieri, A. Cipollone, V. Soma, T. Duguet, and P. Navratil, (2012), arXiv:1211.3315 [nucl-th].
[6] A. Cipollone, C. Barbieri, and P. Navrátil, Phys. Rev. Lett. **111**, 062501 (2013).
[7] K. Tsukiyama, S. K. Bogner, and A. Schwenk, Phys. Rev. Lett. **106**, 222502 (2011).
[8] H. Hergert, S. Binder, A. Calci, J. Langhammer, and R. Roth, Phys. Rev. Lett. **110**, 242501 (2013).
[9] W. H. Dickhoff and C. Barbieri, Prog. Part. Nucl. Phys. **52**, 377 (2004).
[10] A. Rios, A. Polls, and W. H. Dickhoff, Phys. Rev. C **79**, 064308 (2009).
[11] A. Rios and V. Soma, Phys. Rev. Lett. **108**, 012501 (2012).
[12] V. V. der Sluys, D. V. Neck, M. Waroquier, and J. Ryckebusch, Nuclear Physics A **551**, 210 (1993).
[13] A. Idini, F. Barranco, and E. Vigezzi, Phys. Rev. C **85**, 014331 (2012).
[14] V. Somà, T. Duguet, and C. Barbieri, Phys. Rev. C **84**, 064317 (2011).
[15] V. Somà, C. Barbieri, and T. Duguet, Phys. Rev. C **87**, 011303 (2013).
[16] D. V. Neck, M. Waroquier, and J. Ryckebusch, Nuclear Physics A **530**, 347 (1991).
[17] D. V. Neck, M. Waroquier, V. V. der Sluys, and K. Heyde, Nuclear Physics A **563**, 1 (1993).
[18] H. Müther and L. Skouras, Physics Letters B **306**, 201 (1993).
[19] H. Müther and L. Skouras, Nuclear Physics A **581**, 247 (1995).
[20] Y. Dewulf, D. V. Neck, L. V. Daele, and M. Waroquier, Phys. Lett. B **396**, 7 (1997).
[21] D. Van Neck, K. Peirs, and W. M., Jour. Chem. Phys. **115**, 15 (2001).
[22] J. Schirmer and G. Angonoa, J. Chem. Phys. **91**, 1754 (1989).
[23] C. Barbieri and W. H. Dickhoff, Phys. Rev. C **65**, 064313 (2002).
[24] C. Barbieri, Phys. Lett. B **643**, 268 (2006).
[25] C. Barbieri and M. Hjorth-Jensen, Phys. Rev. C **79**, 064313 (2009).
[26] S. Waldecker, C. Barbieri, and W. H. Dickhoff, Phys. Rev. C **84**, 034616 (2011).
[27] L. P. Gorkov, Sov. Phys. JETP **7**, 505 (1958).
[28] D. S. Koltun, Phys. Rev. Lett. **28**, 182 (1972).

[29] T. Duguet, P. Bonche, P. H. Heenen, and J. Meyer, Phys. Rev. **C65**, 014311 (2001).
[30] T. Duguet and G. Hagen, Phys. Rev. C **85**, 034330 (2012).
[31] F. Capuzzi and C. Mahaux, Annals of Physics **245**, 147 (1996).
[32] C. Barbieri and B. K. Jennings, Phys. Rev. C **72**, 014613 (2005).
[33] A. Carbone, A. Cipollone, C. Barbieri, A. Rios, and A. Polls, "Self-consistent Green's functions formalism with three-body interactions," (2013), phys. Rev. C in print, arXiv:1310.3688 [nucl-th].
[34] E. Bergli and M. Hjorth-Jensen, Annals of Physics **326**, 1125 (2011).
[35] M. Brand, K. Allaart, and W. Dickhoff, Physics Letters B **214**, 483 (1988).
[36] J. Yuan, (1994), ph.D thesis, Washington University, St. Louis.
[37] C. Barbieri, D. Van Neck, and W. H. Dickhoff, Phys. Rev. A **76**, 052503 (2007).
[38] D. R. Entem and R. Machleidt, Phys. Rev. C **68**, 041001 (2003).
[39] R. Machleidt and D. R. Entem, Phys. Rep. **503**, 1 (2011).
[40] S. K. Bogner, R. J. Furnstahl, and A. Schwenk, Prog. Part. Nucl. Phys. **65**, 94 (2010).
[41] N. Parlett and D. S. Scott, Math. Comp. **33**, 217 (1979).
[42] E. Caurier, G. Martínez-Pinedo, F. Nowacki, A. Poves, and A. P. Zuker, Rev. Mod. Phys. **77**, 427 (2005).
[43] C. Barbieri, D. Van Neck, and M. Degroote, Phys. Rev. A **85**, 012501 (2012).